Catalyst Deactivation Processes During 1-Hexene Polymerization

Anuj Joshi, Harmen S. Zijlstra, Scott Collins, and J. Scott McIndoe*

Department of Chemistry, University of Victoria, PO Box 1700 STN CSC, Victoria, BC V8W 2Y2, Canada.

Fax: +1 (250) 721-7147; Tel: +1 (250) 721-7181; E-mail: mcindoe@uvic.ca

Abstract

The catalyst $[Cp_2Zr(\mu\text{-}Me)_2AlMe_2]^+[B(C_6F_5)_4]^-$ (**1**) has been studied by electrospray ionisation mass spectrometry (ESI-MS) in order to better understand the complexities of catalyst deactivation in the polymerisation of 1-hexene. Using offline, online and flow-based methods, we observe that zirconium π-allyl species are unstable in solution and previously unobserved dimethylalane complexes are more stable. The dimethylalane complexes are resistant to further 1-hexene additions and their formation represent a new pathway for catalyst deactivation.

Graphical abstract

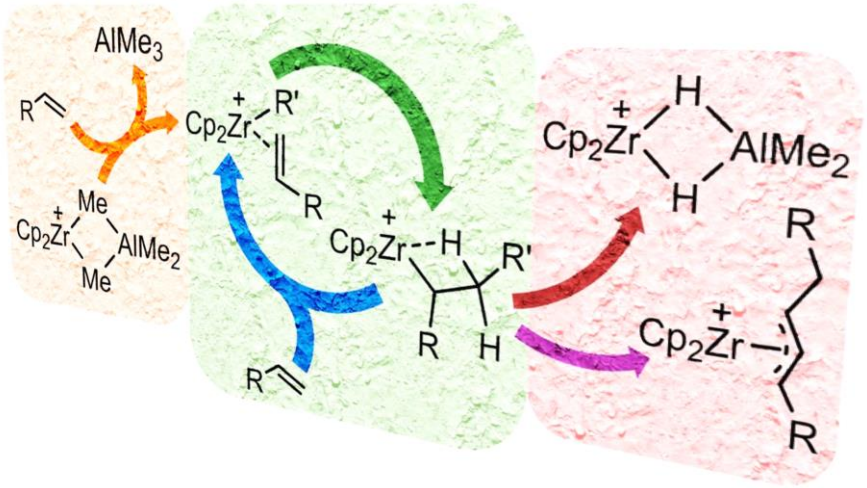

Introduction

In situ monitoring of olefin polymerization,[1] mediated by metallocene or other transition metal catalysts, has emerged as a powerful tool for detection of initiators, resting states and deactivation reactions inherent to these complex catalyst systems.[2] A variety of spectroscopic techniques, including UV-Vis[3] and NMR spectroscopy,[4] have been applied to this problem. Impressive gains in sensitivity have been achieved using NMR and isotopically labelled[5] or hyper-polarized monomer,[6] combined with specialized flow or stopped-flow reactors.[7] NMR spectroscopy remains the definitive method for structural characterization of reactive intermediates,[8] though model compounds are often employed to confirm *in situ* spectroscopic assignments.[9] Mass spectrometric methods have also been employed to study olefin polymerization,[10] with ESI-MS emerging as a sensitive and potent method for both detecting and identifying catalyst intermediates in solution,[11–13] and for studying their reactivity in the gas phase.[14]

These studies have revealed a wealth of information – the nature of the catalyst resting states is dependent on catalyst structure, the method of activation, the nature of the counter-ion, and even monomer.[2] In the case of discrete metallocenium ions, generated *in situ* from metallocene dialkyls and activators such as $B(C_6F_5)_3$ or $[Ph_3C][B(C_6F_5)_4]$, dormant states are π-allyl complexes formed *in situ* via C-H activation of α-olefins or unsaturated chain ends.[15] The extent to which these well-studied complexes are competent for further chain growth is catalyst, counter-ion and monomer dependent.[16,17] In other cases where the (unhindered) metallocene is prone to β-H elimination, dormant contact ion-pairs such as $Cp_2ZrR(\mu\text{-}HB(C_6F_5)_3)$ form using borane-activated catalysts[18] and these can be rather resistant to further insertion.[19]

In MAO-activated metallocenes, where Me_3Al is inevitably present as a chain transfer agent, the π-allyl species are also detected,[20] though their concentration is lower than that of the main, chain-carrying $[Cp_2Zr(\mu\text{-}R)(\mu\text{-}Me)AlMe_2]^+$ complexes identified some time ago by Brintzinger and Babushkin.[5] Further, in MAO-activated systems, the π-allyls appear susceptible to chain transfer to Al[20] and this provides another mechanism for catalyst reactivation.

In other work featuring the use of *i*-Bu_3Al as the alkylating agent/scavenger and $[Ph_3C][B(C_6F_5)_4]$ as activator, π-allyl cations can form *in situ*.[21] However, the principle resting state during polymerization in the case of *i*-Bu_2AlH features $[Cp_2ZrR]$ cations, stabilized by coordination of *i*-Bu_2AlH forming trinuclear Zr,Al_2 complexes with strong Zr-H-Al bridging.[22] Given the presence of *i*-Bu_2AlH in *i*-Bu_3Al solutions, one suspects these intermediates may play a role in olefin polymerization in a catalyst system developed many years ago – *viz.* $Cp_2ZrCl_2/R_3Al/[Ph_3C][B(C_6F_5)_4]$[23] as an alternative to MAO-activated catalysts.[24]

Over the past several years we have applied ESI-MS to the study of MAO-activation of metallocene complexes in fluorobenzene (PhF) solution where both cationic and anionic species can be readily detected and characterized.[25,26] We have also studied ion-speciation in the case of additive such as octamethyltrisiloxane (OMTS) which forms well-defined ion-pairs $[Me_2Al(OMTS)][(MeAlO)_{16}(Me_3Al)_6Me]$ through the process of $[Me_2Al]^+$ abstraction from the MAO.[27] This additive has proven useful in monitoring both aging and oxidation of MAO,[28,29] features known to be important in affecting the efficacy of this elusive but important activator.[30–32]

We have also studied the reaction of MAO-activated Cp_2ZrMe_2 with ethylene in toluene solution at low ethylene pressures.[33] In that case, a hitherto undetected, but long-suspected process for catalyst deactivation[34] was revealed by ESI-MS – formation of inactive, dinuclear Zr_2 complexes arising from the reaction of active species (i.e. $[Cp_2ZrR]^+$) with each other, as shown through experiments with labeled ethylene-d_4.

During that study we briefly explored the use of *in situ* reaction monitoring via pressurized sample infusion (PSI)[35] to study ethylene polymerization in PhF solution using diluted monomer (99:1 ethane:ethylene mixture) as both reactant and pressure source. Considerable difficulty was encountered in pumping dilute MAO solutions via the PSI technique, due to incipient clogging issues (i.e. formation of boehmite gel at the spray tip or along the flow path which included an in-line filter to remove solid PE). These features gave rise to both random and systematic variations in flow rate as well as spray instability arising from the latter. This has a negative effect on the appearance of the total ion chronogram (TIC), which renders collection of reliable kinetic data problematic. We thus decided to focus on 1-hexene polymerization using a MAO-free catalyst system, $Cp_2ZrMe_2/Me_3Al/[Ph_3C][B(C_6F_5)_4]$, which has been previously studied for carbo-alumination of alkenes in some detail by the Norton group.[36]

Results – Catalyst Activation

The synthesis of $[Cp_2Zr(\mu\text{-}Me)_2AlMe_2][B(C_6F_5)_4]$ (**1**) has been described and involves addition of excess Me_3Al to $[Cp_2ZrMe][B(C_6F_5)_4]$ (**2**) generated *in situ* from Cp_2ZrMe_2 and $[Ph_3C][B(C_6F_5)_4]$ at low temperature.[37] High isolated yields are obtained upon subsequent crystallization. However, we wondered whether we could monitor this activation process at room temperature in PhF solvent using ESI-MS. Aside from the use of PhF, this approach mimics what is typically done in olefin polymerization studies – i.e. *in situ* catalyst generation. One basic approach involved simultaneous pumping of a 0.31 mM stock solution of $[Ph_3C][B(C_6F_5)_4]$ in PhF and 0.31 mM stock solutions of Cp_2ZrMe_2 and Me_3Al at different Al:Zr ratios into a mixing tee inside a glove-box with a short length (30 cm) of PTFE tubing running from the tee to the source compartment of the QTOF Micromass spectrometer.

The dead time of this system was about 44 sec at a combined flow rate of 20 µL/min. By varying the flow rate one obtains "snapshots" of the instantaneous product distribution at various time scales in a continuous process. An example of the data obtained is shown in Figure 1. At a 2:1 Al:Zr stoichiometry, formation of $[Cp_2Zr(\mu\text{-}Me)_2AlMe_2]^+$ (**1** *m/z* 307) and the dinuclear complex $[(Cp_2ZrMe)_2(\mu\text{-}Me)]^+$ (**3** *m/z* 485) occur at competitive rates. At longer reaction times, formation of **3** is suppressed as the Cp_2ZrMe_2 is consumed and **2** is competitively trapped by Me_3Al forming **1**. Slow addition of a 1:2 to 1:10 mixture of Cp_2ZrMe_2:$AlMe_3$ to a rapidly stirred solution of $[Ph_3C][B(C_6F_5)_4]$ in PhF (basically titration to a colorless endpoint) gave the cleanest formation of $[Cp_2Zr(\mu\text{-}Me)_2AlMe_2][B(C_6F_5)_4]$ (**1**).

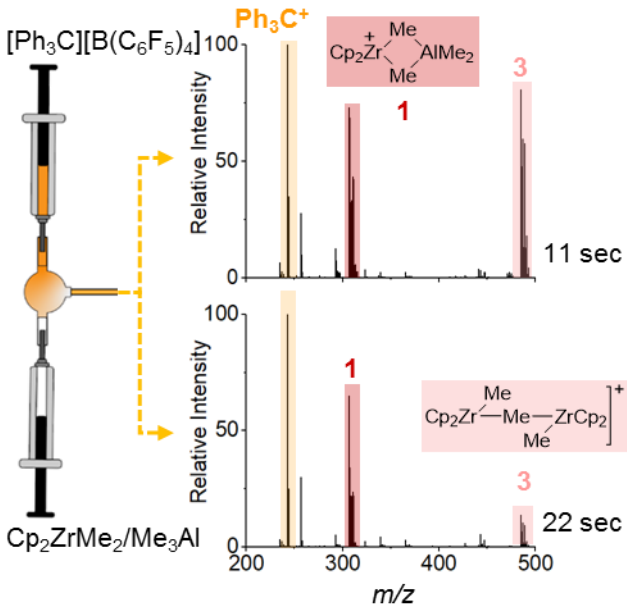

Figure 1 – Monitoring of catalyst activation using $[Ph_3C][B(C_6F_5)_4]$ (0.31 mM), Cp_2ZrMe_2 (0.31 mM) and Me_3Al (0.61 mM). Representative mass spectra after 11 seconds and 22 seconds are shown.

Hexene polymerization experiments were conducted with solutions dominated by **1**, but **3** also reacted with hexene, confirming that both **1**[37] and **3**[38] act as reservoirs of **2**.

We attempted to generate **2** *in situ* by the addition of Cp_2ZrMe_2 to 1 equiv. of $[Ph_3C][B(C_6F_5)_4]$ in PhF. At [Zr] = 4.0 mM the reaction affords a mixture of **2** and **3**. The direct reaction between Cp_2ZrMe_2 and $[Ph_3C][B(C_6F_5)_4]$ is slower in comparison to reactions conducted in the presence of Me_3Al. It is known that competing formation of **3** impedes activation of Cp_2ZrMe_2.[37,38] Trace amounts of a fluorobenzene complex of **2** with *m/z* 331[12,39] were also detected

in this experiment (see Supporting Information Figure S-1). Since the reaction was not clean, and it appears **2** is also unstable in PhF, decomposing to form $[(Cp_2ZrMe)_2(\mu\text{-}F)]^+$ (among other species) over a 3 hour period, we focused much of our subsequent efforts on the reactivity of **1**.

Hexene Polymerization – Monomer Consumption

Hilty and co-workers studied hexene polymerization using **2** in ca. 90:10 toluene:PhF mixtures with [Zr] = 2-19 mM and [hexene] = 0.283 M at room temperature.[6] Using special injection and mixing techniques, involving hyperpolarized monomer, they were able to acquire ^{13}C spectra within 0.45 sec of mixing and estimated k_p = 95 M^{-1} s^{-1} for consumption of monomer over a 12 sec period. They invoked rapid decay of the propagating species under these conditions (from the biexponential decay curves seen for hexene consumption) and concluded that this deactivation process led to π-allyl formation with k_d ~ 0.88 s^{-1}. Hexene consumption is about 30× faster than catalyst deactivation at constant monomer concentration.

On the other hand, Norton and co-workers studied carboalumination of allylbenzene at 40 °C, using $[(EBI)Zr(\mu\text{-}Me)_2AlMe_2][B(C_6F_5)_4]$ (EBI = *rac*-1,2-ethylenebis(η^5-indenyl)) with [Zr] = 0.38 mM, [allylbenzene] = 2.55 mM and a large excess of Me_3Al (>50:1 Al:Zr) with k_{obs} = 5.1×10^{-4} s^{-1} at [Al] = 61 mM corresponding to a second order rate constant of 1.3 M^{-1} s^{-1} for consumption of allylbenzene at this higher temperature. Conventional (NMR) methods were used to monitor this much slower reaction.

Finally, in a very recent study employing UV-Vis spectroscopy, Brintzinger and co-workers studied hexene polymerization using $[(SBI)Zr(\mu\text{-}Me)_2AlMe_2][B(C_6F_5)_4]$ (SBI = *rac*-$Me_2Si(\eta^5\text{-indenyl})_2$) in benzene solution with k_p = 135 M^{-1} s^{-1} and [Zr] = 0. 5 mM. They concluded that the propagating species formed two kinds of π-allyl complexes. Those formed from direct C-H activation of terminal alkenes (including hexene) were unreactive towards further monomer insertion, while those formed from iso-alkenes, formed following β-H elimination, were sluggishly reactive. The latter type also underwent slow reactivation through chain transfer to excess Me_3Al.[17]

We monitored 1-hexene polymerization in PhF solution with [Zr] = 0.25 mM and Al:Zr = 1000:1 at room temperature with [hexene] = 0.25 M by ^1H NMR spectroscopy. A vortex mixture was used to mix catalyst with monomer, where the tube was cooled to -23 °C prior to addition of catalyst. A 30 second delay, corresponding to sample insertion, and locking was required before the first ^1H spectrum could be acquired with the probe at room temperature. Under these conditions, initial monomer consumption was essentially complete by the time the first spectrum was acquired.

In agreement with the results of Hilty, we observed rapid catalyst deactivation evidenced by incomplete conversion of monomer (25-30%). At higher [Zr] = 1.0 mM more extensive consumption of monomer was observed (75% conversion on mixing), and now, a slower process that resulted in additional monomer consumption was detected (data are shown in the Supporting Information Figure S-2 and S-3). This slower process featured k_{obs} = 4.07×10^{-4} s^{-1} or a second order rate constant of 0.41 M^{-1} s^{-1} (roughly 100× slower than initial monomer consumption *vide infra*).

At lower temperature it was possible to monitor the faster monomer consumption step, and though deviation from first order kinetics was observed, consistent with catalyst deactivation, the limiting value for k'_{obs} = 3.1x10^{-4} s^{-1} or k_p = 12.3 M^{-1} s^{-1} at 0 °C (Supporting Information Figures S-4 and S-5). Neglecting any entropic component to the free energy of activation ($\Delta G^{\ddagger}$ = 20 kcal mol^{-1} estimated from the Eyring equation for k'_{obs} at 0 °C), one can estimate that k'_{obs} = 0.0078 s^{-1} at 298 K, which corresponds to a second order propagation rate constant of ca. 31 M^{-1} s^{-1}.

This is lower than the value (95 M^{-1} s^{-1}) determined by Hilty and co-workers for the same catalyst in 90:10 toluene:PhF. The effect of solvent polarity on catalyst activity is dependent on ion-pairing;[40] with strongly ion-paired systems an increase in polarity results in a significant increase.[41] Here, one would expect only modest differences given the weakly coordinating nature of the borate counter-ion but, in any event, an increase rather than a decrease in k_p is anticipated.

On the other hand, Norton and co-workers established that the rate of carboalumination featured an inverse, first order dependence on [Me_3Al] with the concentration of monomeric Me_3Al being governed by the relevant dissociation equilibrium: $Me_6Al_2 \leftrightarrow 2Me_3Al$ with K_d (298 K) = 4.15 × 10^{-6} M.[42] The rate law they derived can be related to the current discussion through the following equation:

$$\text{Rate} = -\frac{d[\text{olefin}]}{dt} = \frac{k_1 k_2 [\text{Zr}][\text{olefin}]}{(k_{-1}+k_2)\left(\frac{[Me_3Al]}{K'}+1\right)} = \frac{k_p[\text{Zr}][\text{olefin}]}{\frac{[Me_3Al]}{K'}+1}$$

where K' is the equilibrium constant for dissociation of monomeric Me_3Al from **1**. At the lower Al concentrations used here (i.e. [Al] = 2.8 mM with monomeric [Me_3Al] = 76 μM) one can estimate from their value of K' at 40 °C (4.1 × 10^{-4} M) that only a slight retardation on insertion rates is expected (ca. 14%). However, one can expect a significant decrease in K' with a decrease in temperature, and thus more significant inhibition by excess Me_3Al at lower temperatures.

Evidently, monomer (and catalyst) consumption occurs at *minimum* initial rates between 0.024 – 2.4 mM s^{-1} at room temperature with [Zr] = 0.28 mM depending on monomer concentration. The slower monomer consumption stage on the other hand is characterized by much more leisurely changes in [Zr] = 0.32-32 μM s^{-1} or 0.019-1.9 mM min^{-1}, and this will be important for interpreting what follows.

Unsaturated Groups in Polyhexene

A ^{1}H NMR spectrum recorded in PhF solution at [Zr] = 4.0 mM following the addition of 100 equiv. of hexene (corresponding to starved feed conditions *vide infra*) was revealing with respect to formation of unsaturated structures in the polyhexene produced (see Supporting Information Figure S-6).

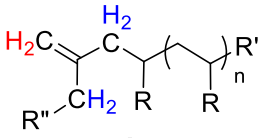

A

0.652*4 = 2.61

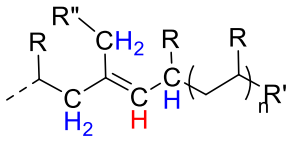

B

0.266*5 = 1.33

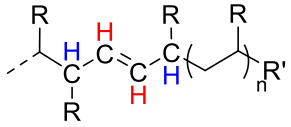

C

0.082*2 = 0.164

Allylic CH:Olefinic CH =
Σ(2.61 + 0.164 + 1.33):1 = 4.10:1

R = n-Bu, R' = H or Me, R"= n-Pr

Chart 1 – Unsaturated groups in poly(hexene)

Signals due to vinylidene ($H_2C=CR_2$), trisubstituted vinyl ($R_2C=CHR$) and vinylene (RCH=CHR)protons are seen in this spectrum in the region 4.6-4.8, 5.1-5.3 and 5.3-5.5, respectively.[43] The ratio of these groups in the polymer is 0.65_2:0.26_6:0.082. Allylic protons are also present, which after correction for the presence of unreacted hexene, integrate to 4.4 protons relative to these olefinic signals. As shown in Chart 1 a ratio of 4.1:1 is expected for the structures **A**-**C**.

Structure **A** corresponds to end groups formed by β-H elimination (or chain transfer to monomer) following primary 1,2-insertion of hexene into $[Cp_2ZrR]^+$ {R = Me, $-(C_6H_{12})_nH$}.[44] Structures **B** and **C** correspond to internal, rather than terminal unsaturation. The accepted mechanism for forming these structures invokes C-H activation (and elimination of H_2) following β-H elimination, forming π-allyl complexes **4** or **5**, followed by further chain growth as shown in Scheme 1.[15–17]

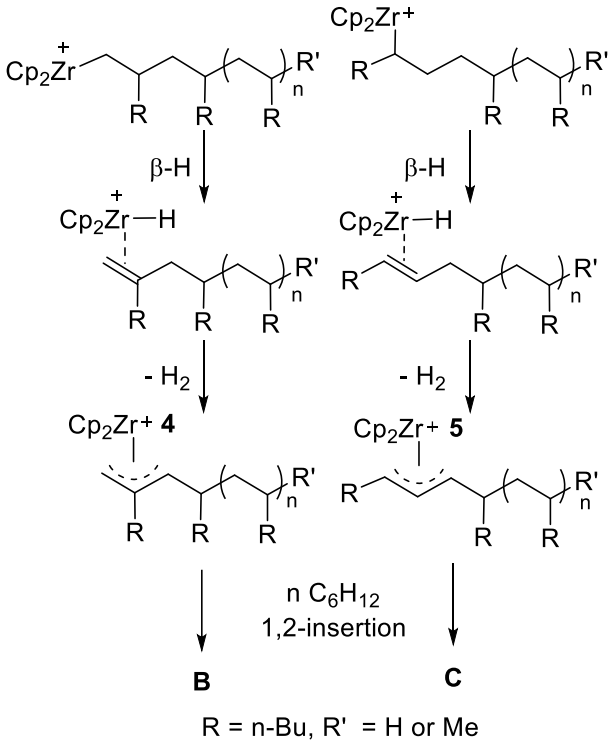

Scheme 1 – Formation of unsaturated groups in poly(hexene)

The predominance of structure **B** over **C** reflects the preference for primary 1,2- vs. secondary 2,1-insertion, coupled with presumably differential reactivity of the resulting π-allyl complexes **4** and **5** towards further insertion. Evidently, under these starved feed conditions, the poly(hexene) formed presents extensive evidence for β-H elimination, coupled with C-H activation. One might expect to observe **4** and **5** during hexene polymerization based on these results.

From the ratio of the vinylidene end groups to the CH protons of the main chain it can be deduced that the average degree of polymerization is close to 5 in this material (M_n = 420 g mol^{-1}). This corresponds to three repeat units of monomer with one saturated and unsaturated end group per chain. The intensity of the vinylidene protons with respect to the main chain (and terminal) Me groups (1:6.4 measured vs. 1:5 calculated) suggest that the majority of chains initiate by insertion into Zr-H (77.5%) vs. Zr-Me (22.5%). Given the 100:1 monomer:Zr ratio, roughly 8 chains are produced per Zr at 38% conversion of monomer in this experiment.

Catalyst Speciation at Steady State – Constant Monomer Concentration

Solutions of activated catalyst [Zr] = 0.28 mM, and a solution of monomer (1000 equiv.) in PhF, each containing Me_3Al ([Al] = 2.8 mM), were simultaneously pumped into the mixing tee referred to earlier. By varying both the flow rate through the tee as well as the hexene:Zr ratio at constant [Al] information is retrieved about the distribution of products at a given time point in a continuous process. While continuous, or semi-continuous (i.e. continuous in monomer, batch in polymer) processes are widespread in commercial application, they are not routinely studied using spectroscopic methods. ESI-MS is ideally suited to that approach and shown in Figure 2 are some representative mass spectra of product mixtures at different reaction times at a 1000:1 hexene:Zr ratio.

Flow rate is a proxy for reaction time, with high flow rates corresponding to a short reaction time before the mixed solution emerges into the ESI-MS source.

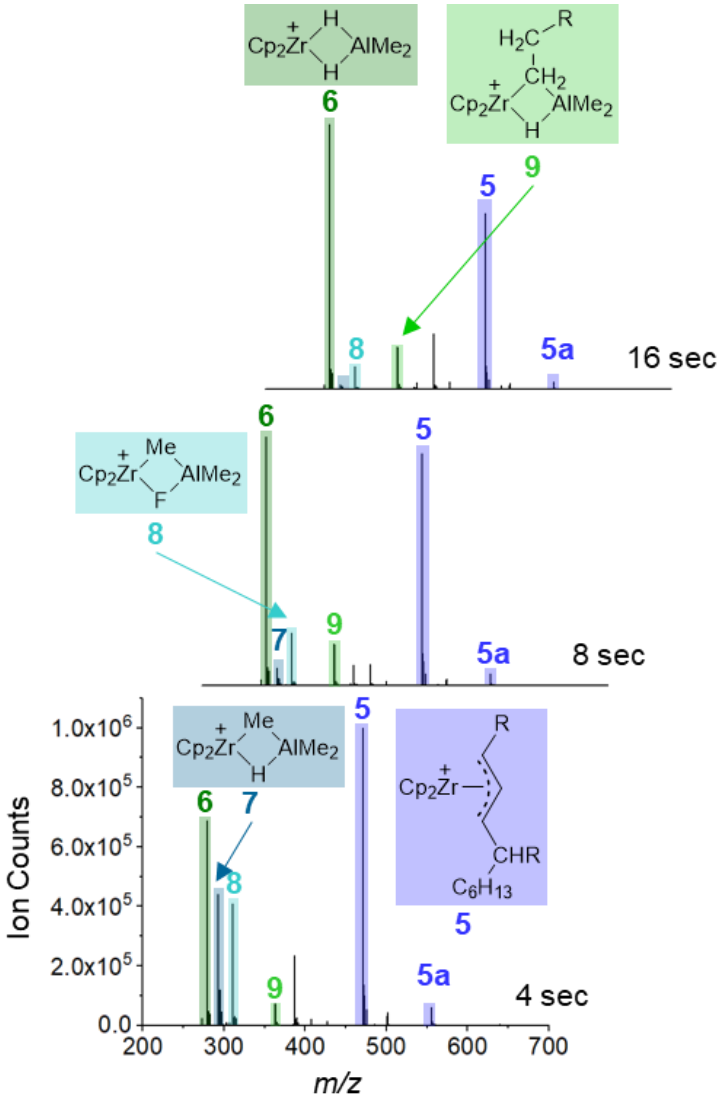

Figure 2 Positive ion ESI-MS of the product ions formed at different reaction times with hexene:Cp_2ZrMe_2 = 1000:1 in PhF ([Zr] = 0.31 mM).

With lag times of 4-16 sec using a 21.5 cm length of tubing, we see a mixture of new ions at *m/z* 279, 293, 311, 363 and 471. In our earlier work,[33] ions with *m/z* 279 and 293 were also formed in PhF solution during PSI experiments involving diluted ethylene. The ion with *m/z* 279 was shown to be $[Cp_2Zr(\mu\text{-}H)_2AlMe_2]$ (hereinafter **6**) on the basis of its MS-MS spectrum, a single loss of 58 Da (Me_2AlH) at low collision energies (Supporting Information Figure S-7).[33] The MS-MS spectrum of *m/z* 293 is dominated by loss of 16 Da (i.e. CH_4) and 72 Da (i.e. Me_3Al) at low collision energies (Supporting Information Figure S-8). One formula for this ion is thus $[Cp_2ZrH(AlMe_3)]^+$ or more probably $[Cp_2Zr(\mu\text{-}H)(\mu\text{-}Me)AlMe_2]^+$ (hereinafter **7**).

The ion with *m/z* 311, which like **7**, is more prominent in the mixture at short reaction times, was also seen in earlier experiments in PhF solution.[33] Since this ion was not observed in ethylene (or hexene) polymerization experiments conducted in toluene solution, it was assigned to $[Cp_2Zr(\mu\text{-}F)(\mu\text{-}Me)AlMe_2]^+$ (**8**) ostensibly a product of C-F activation, a reaction that is known to be mediated by cationic zirconocene complexes in the presence of TiBAl.[45]

The MS-MS spectra of *m/z* 311 is not entirely consistent with this formulation; it readily loses 16 (CH_4) and then 66 Da (C_5H_6) at increased collision energies (Supporting Information Figure S-9). It also loses 72 Da (i.e. Me_3Al) in competition with methane loss (Supporting Information Figure S-10), which is analogous to the behaviour seen with *m/z* 293 (or ion-pair **1**[26]). Though this ion often dominated under starved feed conditions (see e.g. Figure 3 at 4 minutes or Figures 4a-b), it could not be detected in solution using ^{19}F NMR spectroscopy.

Finally, it was observed that the intensity of this ion was maximal upon initial pumping of solutions of ion-pair **1** and hexene. Prolonged pumping of these solutions led to a pronounced decrease in the intensity of this ion relative to the others present (Figure 3). Subsequent pumping of a fresh solution of monomer and catalyst also exhibited low levels of *m/z* 311 suggesting this ion forms from a contaminant in the source compartment (rather than in solution) which is gradually depleted when pumping catalyst + monomer solutions.

Though we are uncertain of its structure, it is evident that it likely forms in the gas phase and involves the reaction of an impurity present with reactive Zr species we do not detect in these experiments as there was no concomitant increase in any of the other product ions. We will discuss these issues later after presentation of all of the data obtained.

The ion with *m/z* 363 fragments with initial loss of 84 Da (i.e. hexene), to form *m/z* 279, followed by a 58 Da loss (Me_2AlH) to form *m/z* 221 $[Cp_2ZrH]^+$ (Supporting Information, Figure S-11). It can thus be formulated as $[Cp_2ZrH_2AlMe_2(hexene)]^+$ (**9**), though it could also correspond to the insertion product $[Cp_2Zr(\mu\text{-}H)(\mu\text{-}n\text{-}C_6H_{13})AlMe_2]^+$.

The relative intensities of *m/z* 363 and 279 were highly variable in this work, and experiments at different cone voltages established that the loss of hexene from 363 occurs at low collision energies, during transit of ions from the source compartment to the high vacuum region of the spectrometer. Even subtle changes in the pressure (and presumably atmospheric composition[46]) within the source compartment had noticeable effects on the ratio of these two ions. Similar effects have been noted before in the case of ion **1**, which generates ion **2** via CID within the source compartment of the mass spectrometer.[26,46] Indeed in those experiments where ion **6** was prominent, the same was true of ion **2** - prior to the introduction of hexene.

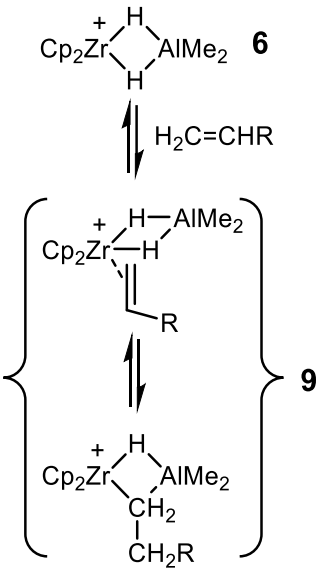

Scheme 2 – Possible equilibria between *m/z* 279 and 363.

When a solution containing **9** was treated with excess *i*-Bu_3Al, substitution of the two Me groups for *i*Bu was observed (substitution of Me by *i*Bu leads to a mass difference of 42 Da), leading to formation of ions with *m/z* 405 and 447 (see Supporting Information Figure S-17). However, no ions corresponding to substitution of a Zr- or Al-hexyl group were observed. This also supports the formulation of ion **9** as indicated above. Note that we cannot exclude the possibility that **6** and **9** are actually in equilibrium with each other through the process of reversible binding of hexene, possibly coupled with reversible insertion (Scheme 2).

The ion with *m/z* 471 was quite resistant to fragmentation by MS-MS. It successively loses 2 Da (i.e. H_2) over the range in collision energies investigated (2-100 V) forming *m/z* 469 and at higher energy *m/z* 467 (Supporting Information Figure S-15 and S-16). Its nominal mass is consistent with the formula $[Cp_2Zr(C_6H_{10})(C_6H_{12})_2H]^+$ and the fact that it is resistant to CID of neutral species is consistent with it being assigned as a π-allyl complex with a formula of $[Cp_2Zr(\eta^3\text{-}C_6H_{10})(C_6H_{12})_2H]^+$ (**5**). A related species with *m/z* 555 was also observed, which given its mass of 84 Da above that of **5** can be assigned as the allyl complex $[Cp_2Zr(\eta^3\text{-}C_6H_{10})(C_6H_{12})_3H]^+$ (**5a**).

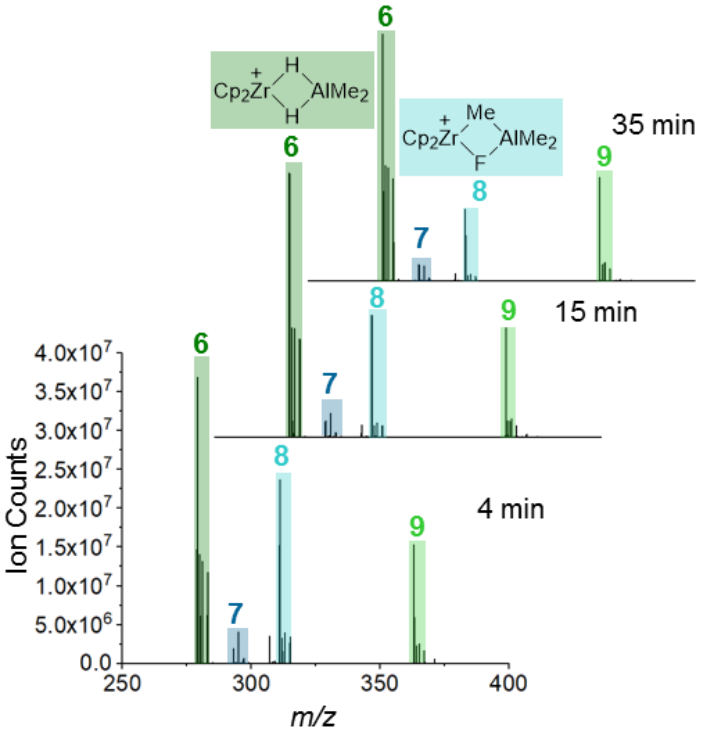

Figure 3 Mass spectra at various times following mixing of $[Cp_2ZrMe_2AlMe_2][B(C_6F_5)_4]$ (**1** [Zr] = 0.31 mM) and monomer with hexene:Zr = 10:1 in PhF.

Catalyst Speciation during Slow Monomer Consumption

To study basic kinetics in more detail requires the study of batch reactions using either off-line, or PSI techniques.[35,47,48] The advantages of the former are convenience and a consistent flow rate (using a syringe pump) while PSI experiments are problematic with respect to flow rate variations in reactions of this type (due to increasing viscosity of the medium and/or incipient clogging issues leading to variations in spray quality). On the other hand, PSI experiments feature lag times that are comparable to those just discussed and allow direct sampling from a reaction vessel. In this work we experienced lag times of ca. 25 sec for a 45 cm length of tubing at 6 psig Ar - see later.

A. Off-line Experiments – 10:1 Hexene:Zr

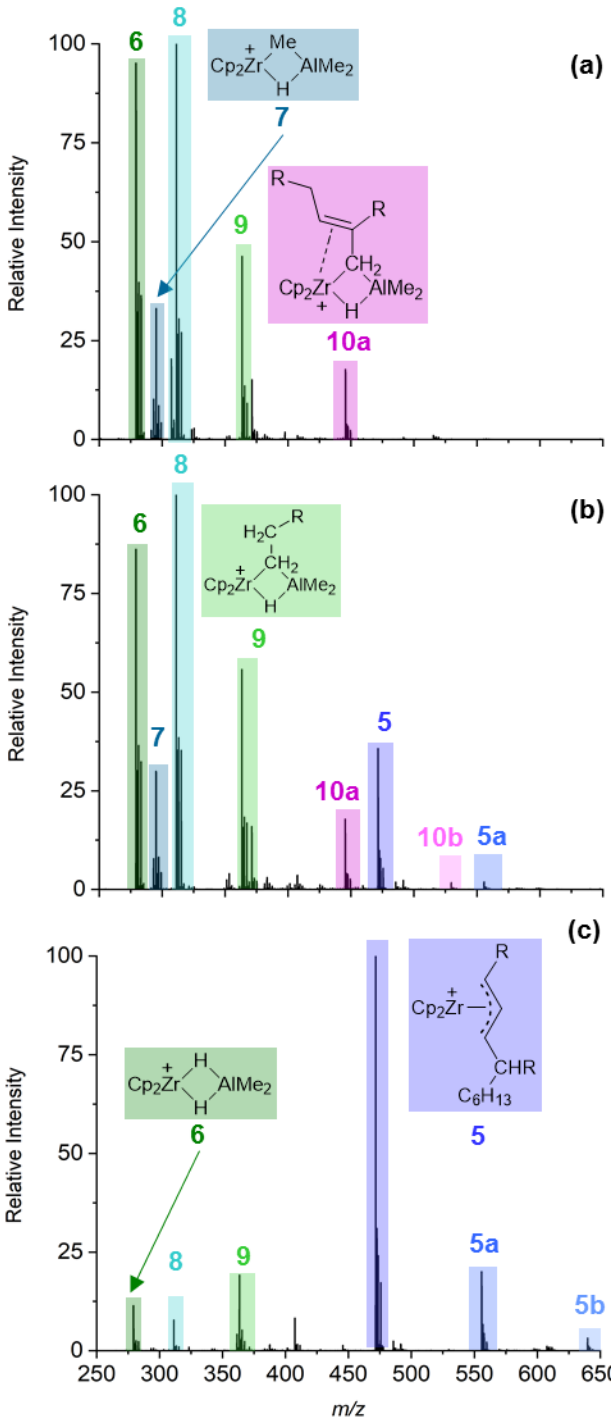

Figure 4 – ESI-MS of reaction mixtures formed from 0.28 mM $[Cp_2ZrMe_2AlMe_2][B(C_6F_5)_4]$ and a) 10 b) 100 and c) 1000 equiv. of hexene in PhF solution. Ions that are separated in mass by 84 Da (C_6H_{12}) are highlighted with different hues of the same color.

Depicted in Figure 4 are representative mass spectra of initial mixtures obtained by adding 10-1000 equiv. of hexene to activated catalyst at [Zr] = 0.28 mM with Me_3Al:Zr = 10:1. As illustrated in Figure 4a), the mixture with 10 equiv. of hexene contains ions **6** - **9**.

Also, an ion with *m/z* 445 (henceforth **10a**), was observed and was much more prominent in off-line experiments compared to the flow experiments discussed previously where it was not detected. Its MS-MS spectrum showed a low energy loss of 58 Da, followed by consecutive losses of 2 Da at higher collision energies (Supporting Information Figures S-12 to S-14). Both lower (*m/z* 361, **10**) and higher homologues at *m/z* 529 (**10b**) and *m/z* 613 (**10c**) were also seen in these experiments though with significantly diminished intensity. Collectively, formation of these products was most noticeable at low monomer:catalyst ratios. Tentatively, these related ions are assigned to the general formula $[Cp_2Zr\{\sigma\text{-}C_6H_{10}(C_6H_{12})_nH\}(\mu\text{-}HAlMe_2)]^+$ (**10**, n = 0; **10a**, *n* = 1; **10b**, *n* = 2; **10c**, *n* = 3) and will be discussed in greater detail later.

B. Off-line Experiments – 1000:1 Hexene:Zr

In experiments featuring a large excess of hexene (i.e. conditions corresponding to polymerization) off-line experiments show predominant formation of ion **5** and higher homologues separated in mass by 84 Da - i.e. **5a**, **5b** etc. (see Figure 4c - these were much more evident in *o*-difluorobenzene which is superior for ESI-MS than PhF but significantly more expensive). The other ions discussed above are also present but in significantly lower amounts (Figure 4c), as might be anticipated from the flow experiment presented earlier.

Though higher homologues were readily detected, lower MW species (i.e. *m/z* 387, 303) were present in essentially trace amounts in these experiments, suggesting formation of **5** is kinetically favoured. In addition to this series of ions, ions differing in mass by +14 Da were seen with weaker and variable intensity (see Supporting Information Figure S-20). These are assigned as analogous π-allyl complexes but involving chains that initiate with Zr-Me vs. Zr-H; they were more prominent at lower monomer:Zr ratios as would be expected.

C. Off-line Experiments – Time Dependent Behavior

While monitoring these off-line experiments as a function of time, we observed that the ions **5**, **5a**, **5b**... were unstable in solution, while ions **10**, **10a**, **10b**... **6**, and **9** appeared to be forming at their expense. Since the isotope distributions of product ions **9** and **10** are incompletely resolved, it was not possible to separately monitor their rate of appearance.

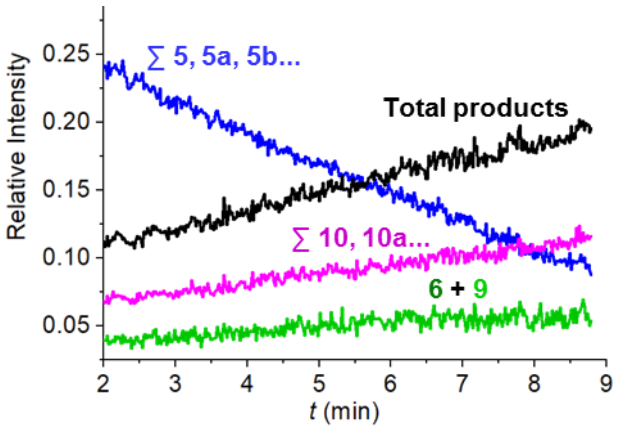

Figure 5 – Sum of normalized ion intensities vs. time for reaction of $[Cp_2ZrMe_2AlMe_2][B(C_6F_5)_4]$ with 1000 equiv. of hexene in PhF.

However, typical data are shown in Figure 5, where we have estimated the rate of formation of **10** from the normalized intensity of its first two isotope peaks, and **9** from its last four isotope peaks, corrected for the complete isotope pattern (see Supporting Information pg. 12 and Figure S-18 for details).

Note that the rate of disappearance of **5**, **5a**, **5b**... is linear with time in this short experiment (ca. 1.5 half-lives). Assuming that the initial normalized intensity represents the fraction of catalyst initially converted to these products (i.e. ca. 25%), the rate of disappearance of these ions corresponds to 0.10 μM s^{-1} which is slower but, in reasonable agreement with the slow process involving monomer consumption discussed earlier. That monomer insertion and subsequent chain transfer (or *vice versa*) involving **5** is necessarily involved in this process is obvious from the fact that the mass distribution of the starting π-allyls (for **5**, **5a**, **5b** X_n = 3, 4, 5...) is greater than that of the products (for **10**, **10a**, **10b**..., X_n = 1, 2, 3... while for **6** and **9**, X_n = 0 and 1).

D. Repetitive Monomer Addition Experiments

Though transient behavior seen in the off-line experiments could correspond to slow monomer consumption seen at higher [Zr], the reactivity of ions **6**, and **9** towards monomer has not been demonstrated and yet these ions are formed at the earliest stages of polymerization, at least under starved feed conditions. We examined this by looking at repetitive additions of hexene to a mixture of these ions using PSI techniques.

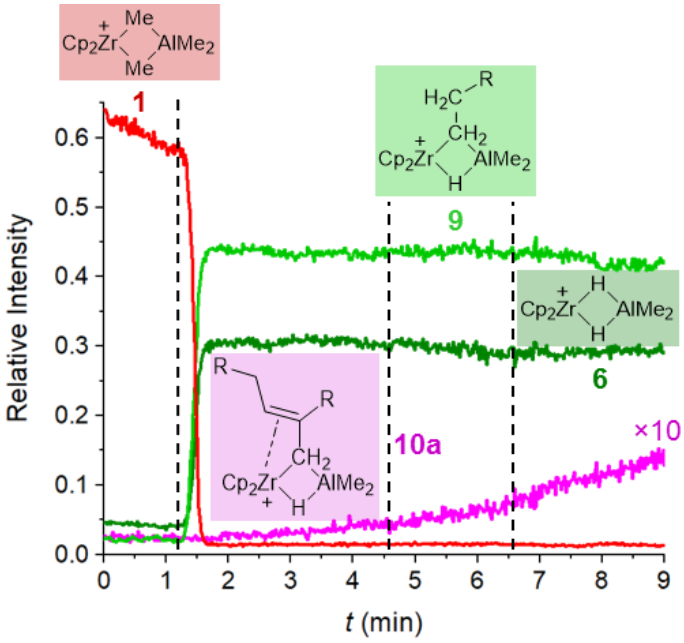

Figure 6 – Normalized ion intensities vs. time for sequential additions of 20 equiv. of hexene to $[Cp_2ZrMe_2AlMe_2][B(C_6F_5)_4]$ (0.25 mM in PhF). Vertical dash lines indicate the additions of hexene, while the intensity of the ion **10a** has been expanded 10-fold.

As shown in Figure 6, addition of 20 equiv. of hexene to a solution of **1** (0.25 mM) led to rapid consumption of this ion with formation of **6** and **9** as the principal products. Further additions of hexene did not lead to consumption (or further growth) of these products, even transiently. During these additions, slow growth of ion **10a** is seen but as it is nearly continuous and unperturbed by the further additions of monomer, it is not obvious that either **6** or **9** are the precursors to this material. That monomer insertion is involved is evident from the higher MW of **10a** relative to either possible precursor. It may be a very unfavourable, pre-equilibrium for dissociation of Me_2AlH from either **6** or **9** that is rate determining in forming **10a.** Similar behavior is exhibited by $[L_2HfH_2Al^iBu_2][B(C_6F_5)_4]$ formed in situ from L_2HfCl_2, excess TiBAl and $[Ph_3C][B(C_6F_5)_4]$ (L_2 = 1,2-C_2H_4(Flu)(5,6-C_3H_6-2-MeInd) on addition of propene.[49]

This experiment shows that formation of **6** and **9** is accompanied by catalyst deactivation, or to be fair, much slower monomer consumption compared to initial rates. Though we hesitate to analyze the build-up of **10a** in this experiment, given the variable monomer concentrations, the pseudo-first order rate constant for this ($k_{obs} \leq 1.4\times10^{-4}$ s^{-1}) is the same order of magnitude as that determined for slow monomer consumption (*vide supra*).

E. Pressurized Sample Infusion Experiments

Initial work of this type focused on the use of PhF as solvent. However, we experienced considerable difficulty using this solvent and this technique, at least within the confines of a glove-box and using a simple apparatus such as that described in the literature.[35] However, better results were obtained using the more polar solvent *o*-difluorobenzene (ε = 13.4, *o*-$C_6H_4F_2$)[50] which is of similar volatility as PhF. Fortunately, the product distributions just discussed in detail were little perturbed by this solvent choice while considerably more intense spectra were seen using this solvent. In Figure 7 are shown two experiments of this type at [Zr] = 0.28 mM with addition of 10 or 1000 equiv. of monomer, with major ions illustrated.

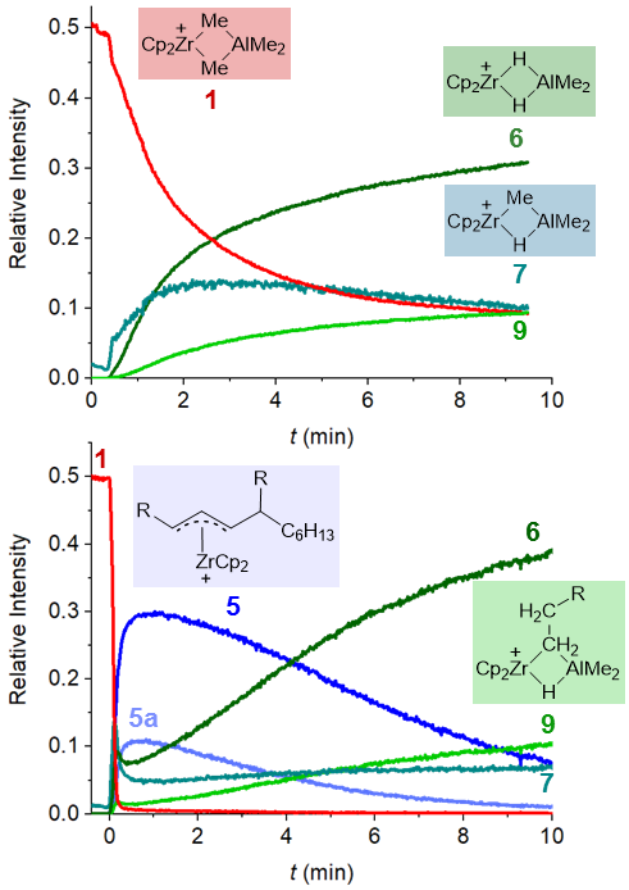

Figure 7 – Normalized ion intensities vs. time for addition of a) 10 equiv. and b) 1000 equiv. of hexene to $[Cp_2ZrMe_2AlMe_2][B(C_6F_5)_4]$ in PhF_2 with [Zr] = 0.28 mM.

Note that in Figure 7a consumption of ion **1** is incomplete. This is expected as dissociation of Me_3Al from this ion is less favourable than for higher analogues[36] while ion-pairing in the resulting 14 e species is expected to be tighter as well, leading to the well-known phenomenon that the first insertion of monomer (with rate constant k_i) is generally quite a bit slower than subsequent insertions.[15,44]

In fact, from Figure 7a, where conversion of ion **1** is ca. 80% and using the equation $n = -(k_p/k_i)\ln([Zr]/[Zr]_o) - (1-(k_p/k_i))[([Zr]/[Zr]_o)-1]$ where n = # equiv. of monomer added,[51] we can estimate that $k_p/k_i = 11$. Also, the limiting slope for this curve at t = 0 corresponds to an initial insertion rate constant of $k_i = 3.3\ M^{-1}\ s^{-1}$. This gives an estimate of $k_p = 36\ M^{-1}\ s^{-1}$ which is in reasonable agreement with that estimated from extrapolation from NMR data at 0 °C for rapid monomer consumption.

Note the initial appearance of ion **7** in Figure 7a along with *m/z* 311 (**8** - not shown as it isotopomer distribution overlaps with that of ion pair **1**). Both of these ions appear at the earliest times in these PSI experiments, consistent with them forming most rapidly from starting material (see also Figure 2). Under starved feed conditions, evidently **7** is the primary product formed, while formation of ions **6** and **9** involve additional steps. In particular, complex **7** might form directly from $[Cp_2Zr(\mu\text{-}R)(\mu\text{-}Me)AlMe_2]$ via β-H elimination, supposing that the propagating ions in this case are the same as those identified by NMR quite some time ago by Brintzinger and co-workers.[5]

The second experiment at 1000:1 monomer to catalyst ratios exhibits a plethora of transient behavior at both short and long time length scales, fully consistent with all prior experiments. Basically, the rapid formation of **7**

(and **8**), subsequent formation of ions **6** and **9**, concomitant formation and subsequent disappearance of ion **5** and homologues (**5a**, **5b** etc.) are beautifully illustrated in this experiment.

It is very clear from these two experiments that the π-allyl complexes **5** only form in the presence of a large excess of hexene, and at a time scale that is similar to formation of **6** and **9** under these conditions. They clearly transform under longer time scales to **6** and **9** in this experiment where we have shown that these two ions are basically unreactive towards monomer.

The kinetic behavior seen in this experiment is strongly reminiscent of that recently reported by Brintzinger and co-workers under similar conditions;[17] rapid consumption of the starting ion-pair with π-allyl intermediates detected at both short and long time scales by UV-Vis spectroscopy. Though we have not monitored these reactions by UV-Vis spectroscopy, there is an obvious color change (to pale orange yellow) upon adding monomer to $[Cp_2ZrMe_2AlMe_2][B(C_6F_5)_4]$ (which is basically colorless), and though this color persists during the PSI experiment, the final solutions (which contain very little **5**) are colorless.

Their basic conclusion was that π-allyl complexes are forming at both of these time scales with some competent for further insertion vs. relatively unreactive. In their work they also observed species at short time scales which they assigned to the 14 e propagating alkyls $[(SBI)ZrR]^+$, though their presence was deduced from deconvolution of the observed spectra, rather than direct observation.

In our case, we do not detect these species via ESI MS and we believe that in the case of hexene, they are just too prone to β-H elimination (forming **7**) or reactive towards impurities (forming **8**) in the source compartment. However, we suspect the time dependence of these ions does closely track with the propagating ions and this accounts for the PSI or other results obtained at short reaction times (Figure 2, see also Supporting Information pg. 13 and Figures S-21 to S-22).

Finally, as shown in Figure 8, under starved feed conditions (i.e. 10 equiv. of monomer), the formation of ions **10a**, **10b** etc. can be detected, along with ions at m/z 375, 459, 543...with the latter more intense than the former, at least initially. The ion with m/z 361 (**10**) is not detected with significant intensity in this PSI experiment but is evident when larger amounts of monomer are added initially (Figure 5). The ion with m/z 459 (thenceforth **10a'**) forms directly during consumption of **1** while there is a distinct lag phase in forming **10a**. As the ion series **10'**... differs from the "parent" series of **10** by +14 Da, it is probable that these ions form by insertion of hexene into Zr-Me vs. Zr-H.

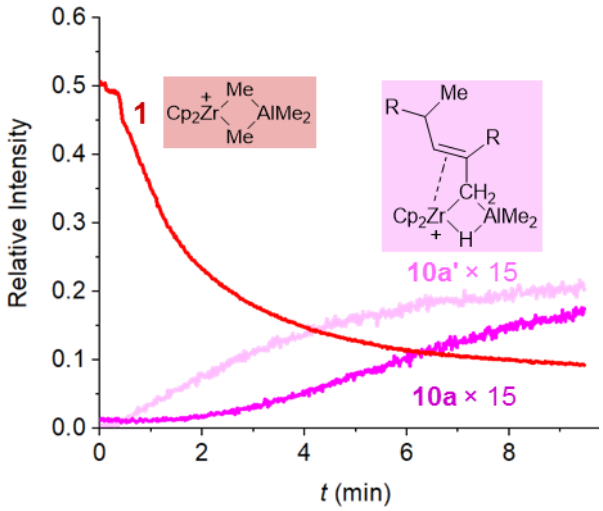

Figure 8 – Normalized ion intensities vs. time for addition of 10 equiv. of hexene to $[Cp_2ZrMe_2AlMe_2][B(C_6F_5)_4]$ in PhF_2 with [Zr] = 0.28 mM. The intensities of ions **10a** and **10a'** are expanded 15-fold, while **1** is not expanded.

Discussion

The formation of ions featuring coordinated Me_2AlH (i.e. **6**, **7**, **9**, and **10**, **10a** and homologues) in these experiments and at the earliest stages of polymerization is without precedent as far as we are aware. That Me_2AlH would strongly bind to a 14 e metal alkyl or hydride is not surprising.[22,49] Efficient trapping of a π-allyl complex to form **10**, **10a**, etc. seems less likely but can't be excluded; trapping of an unobserved $[Ph_2C(Flu)(Cp)Zr(\eta^3\text{-}(H_2C)_2CMe)][B(C_6F_5)_4]$ intermediate by DiBAlH was invoked as a possible mechanism for forming $[Ph_2C(Flu)(Cp)Zr(\mu\text{-}H\text{-}Al^iBu_2CH_2(\eta\text{-}C(Me)=CH_2)][B(C_6F_5)_4]$ *in situ* from $Ph_2C(Flu)(Cp)ZrCl_2$, excess TiBAl and $[PhNHMe_2][B(C_6F_5)_4]$.[52]

Given that ions such as **6** and **9** are resistant to further insertion, their predominant formation under starved feed conditions represents a hitherto unappreciated mechanism for catalyst deactivation or dormancy.

In order to generate Me_2AlH in solution, a propagating intermediate would have to undergo β-H elimination, trapping of $[Cp_2ZrH]^+$ by Me_3Al to form ion **7** which we do observe, and regeneration of $[Cp_2ZrMe]^+$ with release of Me_2AlH (which we do not observe). The latter step seems unlikely, as Me_2AlH is strongly associated under all conditions in solution; the monomeric form has not even been detected in gas phase.[53]

The association of monomeric R_2AlH into higher oligomers has been studied theoretically.[54] For R = *i*-Bu, formation of e.g. dimer from monomer has ΔG = -20.8 kcal mol^{-1} at 298 K in toluene while the cyclic trimer is the most stable form. From this paper, and based on the calculated enthalpy change for R = Me, which is nearly identical, (Me_2AlH is also trimeric in solution[53]) one can estimate that monomeric $[Me_2AlH] \sim 10^{-10}$ M under the conditions studied here.

If we consider the behavior shown in e.g. Figure 5 where formation of ions **6**, **9**, **10** and homologues involves trapping of various 14- or 16e- species by Me_2AlH, the cumulative rate of these processes is ca. 10^{-7} M s^{-1}. If we divide this through by the average concentration of these species (ca. 0.042 mM), and the equilibrium concentration of monomeric Me_2AlH, the estimated second order rate constant for trapping is 2.4×10^8 M^{-1} s^{-1} assuming that process is rate-determining. This in turn implies that any preceding steps involved in forming e.g. $[Cp_2ZrH]^+$ (or π-allyls) are faster, including β-H elimination or C-H activation.

There is simply no precedent for this – the rates of these chain transfer or deactivation processes are certainly slower than propagation (10^2-10^3 M^{-1} s^{-1}). This means trapping cannot be rate determining; a more likely scenario is where initial insertion into **6** or **9** (leading eventually to e.g. a π-allyl complex) is rate limiting due to e.g. an unfavourable equilibrium for dissociation of Me_2AlH. It can be shown, subject to the steady state approximation for any intermediates, that the rate of σ–allyl **10** formation in Figure 5 will be governed by the rate law shown below:

$$\frac{d[\sigma\text{-allyl } \mathbf{10}]}{dt} = k_i K \frac{[\mathbf{6}][C_6H_{12}]}{[Me_2AlH]}$$

where k_i is the rate of insertion of monomer into Zr-H, while K is the equilibrium governing dissociation of Me_2AlH from **6**. Of course, we don't know what K is, though it is reasonable to expect it is similar in magnitude for dissociation of $(Me_2AlH)_2$. Under that assumption one can estimate that k_i = 290 M^{-1} s^{-1} which is larger than that for insertion of hexene into Zr-R (31-36 M^{-1} s^{-1} here or 100-150 M^{-1} s^{-1} under other conditions). That insertion into Zr-H is faster than for Zr-R seems reasonable and the very unfavourable pre-equilibrium [K = 5.8 10^{-16} M for $(Me_2AlH)_2$][54] accounts for the apparent lack of reactivity of ions like **6** towards repetitive additions of hexene.

How are we to interpret the behavior seen under more conventional conditions – as in Figure 7b? Evidently, ions such as **6**-**9** are transiently formed, perhaps in part due to inefficient mixing in either experiment. PSI or off-line experiments where activated catalyst was added last to efficiently stirred monomer solutions, showed consistently lower levels of these ions (see Supporting Information Figure S-19).

However, the main kinetic event features formation of π-allyls **5**. These then undergo slow reaction to ironically form Me_2AlH complexes at longer time scales. Note that this does not involve direct trapping by Me_2AlH as that should form a series of ions with *m/z* 529, 613, 697.... These ions are seen at long reaction times but the dominant member of that series has *m/z* 445 (**10a**) and starts with *m/z* 361 (**10**).

Further, why is formation of **5** predominant vs. lower homologues? With reference to Scheme 1 this is not expected if these π-allyl complexes are of type **4**. It makes perfect sense however if they are of type **5**. Basically, following primary insertion of monomer into Zr-H, it is well known that the next insertion is also highly regioregular, while 2,1-insertion into branched alkyls occurs competitively with 1,2-insertion, especially with aspecific metallocene catalysts.[15,44] The resulting "dormant" state[55] might be expected to undergo competitive β-H elimination and C-H activation (with liberation of H_2) forming selectively **5** and higher homologues.

In the recent work of Brintzinger and co-workers it was proposed that insertion and direct C-H activation of monomer (or chains with terminal vinyl groups – which we do not see here) are competitive events.[17] We see no evidence for this, or if it occurs, the resulting π-allyls (with *m/z* 303, 387 etc.) would have to be efficiently trapped by free Me_2AlH to form ions we do detect (i.e. **10** with *m/z* 361, 445, 529 etc.).

However, the M+14 analogues of these ions (i.e. **10'**) do form at a faster initial rate and directly during consumption of **1** under starved feed conditions. Further, this series of ions **10'** starts with *m/z* 375 while those that feature insertion into Zr-H (i.e. following chain transfer) start at *m/z* 445 (**10a**). It is therefore likely that these σ-allyls form following β-H elimination, and specifically following primary insertion into Zr-R as shown in Scheme 3.

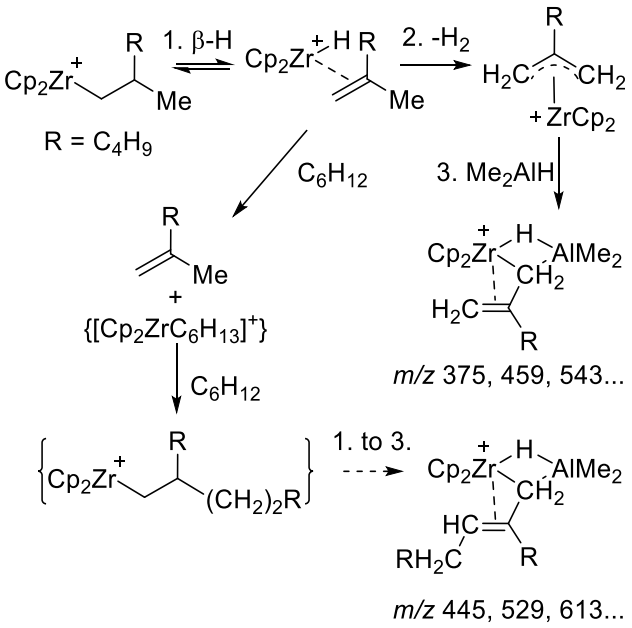

Scheme 3 – Formation of ions with *m/z* 445, 529, 613 vs. 375, 459, 543...

Tentatively, it would appear that π-allyls that feature at least one terminal CH_2 group are efficiently trapped by Me_2AlH while those that don't (**5** with *m/z* 471, 555, 639...) are not. This makes some sense from the perspective of the structures shown in Scheme 3 vs. Scheme 1.

Conclusions

ESI-MS studies of hexene polymerization using $[Cp_2ZrMe_2AlMe_2][B(C_6F_5)_4]$ reveal unanticipated complexity, and identification of a new pathway for catalyst deactivation – formation of dimethylalane stabilized complexes which are resistant to further insertion. Ironically these complexes also form under starved feed conditions, or under any conditions that lead to this condition, such as poor mixing. On the other hand π-allyl complexes dominate under other conditions and our work suggests they have the more hindered structure shown in Scheme 1 (type **5**), and form following 2,1-insertion. We believe they are responsible for slow monomer consumption seen with this catalyst, and that eventually all of the added catalyst pools in dormant or deactivated dimethylalane-stabilized complexes.

Acknowledgements

J.S.M. thanks NSERC (Strategic Project Grant #478998-15) and NOVA Chemicals' Centre for Applied Research for operational funding and CFI, BCKDF, and the University of Victoria for infrastructural support. S.C. acknowledges support for a Visiting Scientist position from the University of Victoria.

References

(1) Haven, J. J.; Junkers, T. Online Monitoring of Polymerizations: Current Status. *European J. Org. Chem.* **2017**, *2017* (44), 6474–6482. https://doi.org/10.1002/ejoc.201700851.

(2) Bochmann, M. The Chemistry of Catalyst Activation: The Case of Group 4 Polymerization Catalysts. *Organometallics* **2010**, *29* (21), 4711–4740. https://doi.org/10.1021/om1004447.

(3) Babushkin, D. E.; Panchenko, V. N.; Brintzinger, H.-H. Zirconium Allyl Complexes as Participants in Zirconocene-Catalyzed α-Olefin Polymerizations. *Angew. Chemie Int. Ed.* **2014**, *53* (36), 9645–9649. https://doi.org/doi:10.1002/anie.201403673.

(4) Christianson, M. D.; Landis, C. R. Generalized Treatment of NMR Spectra for Rapid Chemical Reactions. *Concepts Magn. Reson. Part A* **2007**, *30A* (4), 165–183. https://doi.org/doi:10.1002/cmr.a.20090.

(5) Babushkin, D. E.; Brintzinger, H. H. Reactive Intermediates Formed During Olefin Polymerization by Methylalumoxane-Activated Ansa-Zirconocene Catalysts: Identification of a Chain-Carrying Intermediate by NMR Methods. *J. Am. Chem. Soc.* **2010**, *132* (2), 452–453. https://doi.org/10.1021/ja909157r.

(6) Chen, C.-H.; Shih, W.-C.; Hilty, C. In Situ Determination of Tacticity, Deactivation, and Kinetics in [Rac-(C2H4(1-Indenyl)2)ZrMe][B(C6F5)4] and [Cp2ZrMe][B(C6F5)4]-Catalyzed Polymerization of 1-Hexene Using 13C Hyperpolarized NMR. *J. Am. Chem. Soc.* **2015**, *137* (21), 6965–6971. https://doi.org/10.1021/jacs.5b04479.

(7) Christianson, M. D.; Tan, E. H. P.; Landis, C. R. Stopped-Flow NMR: Determining the Kinetics of [Rac-(C2H4(1-Indenyl)2)ZrMe][MeB(C6F5)3]-Catalyzed Polymerization of 1-Hexene by Direct Observation. *J. Am. Chem. Soc.* **2010**, *132* (33), 11461–11463. https://doi.org/10.1021/ja105107y.

(8) Landis, C. R.; Christianson, M. D. Metallocene-Catalyzed Alkene Polymerization and the Observation of Zr-Allyls. *Proc. Natl. Acad. Sci.* **2006**, *103* (42), 15349–15354. https://doi.org/10.1073/pnas.0602704103.

(9) Vatamanu, M.; Stojcevic, G.; Baird, M. C. Detection of an η-Alkene Intermediate of the Type [Cp2Zr(Me)(H1-Alkene)]+: The Role of Such Species in Metallocene Catalyst Deactivation to Allylic Species. *J. Am. Chem. Soc.* **2008**, *130* (2), 454–456. https://doi.org/10.1021/ja0742683.

(10) Gies, A. P.; Kuhlman, R. L.; Zuccaccia, C.; Macchioni, A.; Keaton, R. J. Mass Spectrometric Mechanistic Investigation of Ligand Modification in Hafnocene-Catalyzed Olefin Polymerization. *Organometallics* **2017**, *36* (18), 3443–3455. https://doi.org/10.1021/acs.organomet.7b00293.

(11) Vatamanu, M. Observation of Zirconium Allyl Species Formed during Zirconocene-Catalyzed Propene Polymerization and Mechanistic Insights. *J. Catal.* **2015**, *323*, 112–120. https://doi.org/https://doi.org/10.1016/j.jcat.2014.12.004.

(12) Jiang, J.; Zhang, H.; Li, M.; Dulay, M. T.; Ingram, A. J.; Li, N.; You, H.; Zare, R. N. Droplet Spray Ionization from a Glass Microscope Slide: Real-Time Monitoring of Ethylene Polymerization. *Anal. Chem.* **2015**, *87* (16), 8057–8062. https://doi.org/10.1021/acs.analchem.5b02390.

(13) Santos, L. S.; Metzger, J. O. Study of Homogeneously Catalyzed Ziegler–Natta Polymerization of Ethene by ESI-MS. *Angew. Chemie Int. Ed.* **2006**, *45* (6), 977–981. https://doi.org/doi:10.1002/anie.200503307.

(14) Feichtinger, D.; Plattner, D. A.; Chen, P. Ziegler−Natta-like Olefin Oligomerization by Alkylzirconocene Cations in an Electrospray Ionization Tandem Mass Spectrometer. *J. Am. Chem. Soc.* **1998**, *120* (28), 7125–7126. https://doi.org/10.1021/ja980004s.

(15) Resconi, L.; Cavallo, L.; Fait, A.; Piemontesi, F. Selectivity in Propene Polymerization with Metallocene Catalysts. *Chem. Rev.* **2000**, *100* (4), 1253–1346. https://doi.org/10.1021/cr9804691.

(16) Lieber, S.; Prosenc, M.-H.; Brintzinger, H.-H. Zirconocene Allyl Complexes: Dynamics in Solution, Reaction with Aluminum Alkyls, B(C6F5)3-Induced Propene Insertion, and Density-Functional Calculations on Possible Formation and Reaction Pathways. *Organometallics* **2000**, *19* (4), 377–387. https://doi.org/10.1021/om9906058.

(17) Panchenko, V. N.; Babushkin, D. E.; Bercaw, J. E.; Brintzinger, H. H. Catalyst Speciation during Ansa-Zirconocene-Catalyzed Polymerization of 1-Hexene Studied by UV-Vis Spectroscopy—Formation and Partial Re-Activation of Zr-Allyl Intermediates †. *Polymers (Basel).* **2019**, *11* (6). https://doi.org/10.3390/polym11060936.

(18) Al-Humydi, A.; Garrison, J. C.; Mohammed, M.; Youngs, W. J.; Collins, S. Propene Polymerization Using Ansa-Metallocenium Ions: Catalyst Deactivation Processes during Monomer Consumption and Molecular Structures of the Products Formed. *Polyhedron* **2005**, *24* (11), 1234–1249. https://doi.org/https://doi.org/10.1016/j.poly.2005.02.005.

(19) Moscato, B. M.; Zhu, B.; Landis, C. R. Mechanistic Investigations into the Behavior of a Labeled Zirconocene Polymerization Catalyst. *Organometallics* **2012**, *31* (5), 2097–2107. https://doi.org/10.1021/om3000955.

(20) Panchenko, V. N.; Babushkin, D. E.; Brintzinger, H. H. Zirconium-Allyl Complexes as Resting States in Zirconocene-Catalyzed α-Olefin Polymerization. *Macromol. Rapid Commun.* **2015**, *36* (2), 249–253. https://doi.org/doi:10.1002/marc.201400444.

(21) Bryliakov, K. P.; Talsi, E. P.; Semikolenova, N. V; Zakharov, V. A.; Brand, J.; Alonso-Moreno, C.; Bochmann, M. Formation and Structures of Cationic Zirconium Complexes in Ternary Systems Rac-(SBI)ZrX2/AlBu3i/[CPh3][B(C6F5)4] (X=Cl, Me). *J. Organomet. Chem.* **2007**, *692* (4), 859–868. https://doi.org/https://doi.org/10.1016/j.jorganchem.2006.10.037.

(22) Baldwin, S. M.; Bercaw, J. E.; Henling, L. M.; Day, M. W.; Brintzinger, H. H. Cationic Alkylaluminum-Complexed Zirconocene Hydrides: NMR-Spectroscopic Identification, Crystallographic Structure Determination, and Interconversion with Other Zirconocene Cations. *J. Am. Chem. Soc.* **2011**, *133* (6), 1805–1813. https://doi.org/10.1021/ja1050428.

(23) Ewen, J. A.; Elder, M. J. Syntheses and Models for Stereospecific Metallocenes. *Makromol. Chemie. Macromol. Symp.* **1993**, *66* (1), 179–190. https://doi.org/10.1002/masy.19930660116.

(24) Chien, J. C. W.; Tsai, W. M.; Rausch, M. D. Isospecific Polymerization of Propylene Catalyzed by Rac-Ethylenebis(Indenyl)Methylzirconium Cation. *J. Am. Chem. Soc.* **1991**, *113* (22), 8570–8571. https://doi.org/10.1021/ja00022a081.

(25) Trefz, T. K.; Henderson, M. A.; Wang, M. Y.; Collins, S.; McIndoe, J. S. Mass Spectrometric Characterization of Methylaluminoxane. *Organometallics* **2013**, *32* (11), 3149–3152. https://doi.org/10.1021/om400256f.

(26) Trefz, T. K.; Henderson, M. A.; Linnolahti, M.; Collins, S.; McIndoe, J. S. Mass Spectrometric Characterization of Methylaluminoxane-Activated Metallocene Complexes. *Chem. – A Eur. J.* **2015**, *21* (7), 2980–2991. https://doi.org/10.1002/chem.201405319.

(27) Zijlstra, H. S.; Linnolahti, M.; Collins, S.; McIndoe, J. S. Additive and Aging Effects on Methylalumoxane Oligomers. *Organometallics* **2017**. https://doi.org/10.1021/acs.organomet.7b00153.

(28) Zijlstra, H. S.; Collins, S.; McIndoe, J. S. Oxidation of Methylalumoxane Oligomers. *Chem. - A Eur. J.* **2018**. https://doi.org/10.1002/chem.201705458.

(29) Endres, E.; Zijlstra, H. S.; Collins, S.; McIndoe, J. S.; Linnolahti, M. Oxidation of Methylalumoxane

Oligomers: A Theoretical Study Guided by Mass Spectrometry. *Organometallics* **2018**, *37* (21), 3936–3942. https://doi.org/10.1021/acs.organomet.8b00587.

(30) Zijlstra, H. S.; Harder, S. Methylalumoxane - History, Production, Properties, and Applications. *European Journal of Inorganic Chemistry*. Wiley-VCH Verlag January 1, 2015, pp 19–43. https://doi.org/10.1002/ejic.201402978.

(31) Z Velthoen, M. E.; Mun, A.; Bouhmadi, A.; Diefenbach, S.; Weckhuysen, B. M. The Multifaceted Role of Methylaluminoxane in Metallocene-Based Olefin Polymerization Catalysis The Influence of Supporting The. *Macromolecules* **2018**, *51*, 54. https://doi.org/10.1021/acs.macromol.7b02169.

(32) Kilpatrick, A. F. R.; Rees, N. H.; Sripothongnak, S.; Buffet, J.-C.; O'hare, D. Slurry-Phase Ethylene Polymerization Using Pentafluorophenyl-and Pentafluorophenoxy-Modified Solid Polymethylaluminoxanes. **2017**. https://doi.org/10.1021/acs.organomet.7b00846.

(33) Collins, S.; Linnolahti, M.; Zamora, M. G.; Zijlstra, H. S.; Rodríguez Hernández, M. T.; Perez-Camacho, O. Activation of Cp2ZrX2 (X = Me, Cl) by Methylaluminoxane As Studied by Electrospray Ionization Mass Spectrometry: Relationship to Polymerization Catalysis. *Macromolecules* **2017**, *50* (22), 8871–8884. https://doi.org/10.1021/acs.macromol.7b00933.

(34) Lancaster, S. J.; Robinson, O. B.; Bochmann, M.; Coles, S. J.; Hursthouse, M. B. Synthesis and Reactivity of New Mono(Cyclopentadienyl)Zirconium and -Hafnium Alkyl Complexes. Crystal and Molecular Structure of [{C5H3(SiMe3)2}HfMe2(.Eta.6-Toluene)][BMe(C6F5)3]. *Organometallics* **1995**, *14* (5), 2456–2462. https://doi.org/10.1021/om00005a049.

(35) Vikse, K. L.; Woods, M. P.; McIndoe, J. S. Pressurized Sample Infusion for the Continuous Analysis of Air- And Moisture-Sensitive Reactions Using Electrospray Ionization Mass Spectrometry. *Organometallics* **2010**, *29* (23), 6615–6618. https://doi.org/10.1021/om1008082.

(36) Camara, J. M.; Petros, R. A.; Norton, J. R. Zirconium-Catalyzed Carboalumination of α-Olefins and Chain Growth of Aluminum Alkyls: Kinetics and Mechanism. *J. Am. Chem. Soc.* **2011**, *133* (14), 5263–5273. https://doi.org/10.1021/ja104032w.

(37) Bochmann, M.; Lancaster, S. J. Monomer–Dimer Equilibria in Homo- and Heterodinuclear Cationic Alkylzirconium Complexes and Their Role in Polymerization Catalysis. *Angew. Chemie Int. Ed. English* **1994**, *33* (1516), 1634–1637. https://doi.org/10.1002/anie.199416341.

(38) Beck, S.; Prosenc, M.-H.; Brintzinger, H.-H.; Goretzki, R.; Herfert, N.; Fink, G. Binuclear Zirconocene Cations with μ-CH3-Bridges in Homogeneous Ziegler-Natta Catalyst Systems. *J. Mol. Catal. A Chem.* **1996**, *111* (1), 67–79. https://doi.org/https://doi.org/10.1016/1381-1169(96)00168-9.

(39) Wu, F.; Dash, A. K.; Jordan, R. F. Structures and Reactivity of Zr(IV) Chlorobenzene Complexes. *J. Am. Chem. Soc.* **2004**, *126* (47), 15360–15361. https://doi.org/10.1021/ja044303v.

(40) Yang, S. H.; Huh, J.; Jo, W. H. Effect of Solvent Polarity on the Initiation and the Propagation of Ethylene Polymerization with Constrained Geometry Catalyst/MAO Catalytic System: A Density Functional Study with the Conductor-like Screening Model. *Macromolecules* **2005**, *38* (4), 1402–1409. https://doi.org/10.1021/ma0481961.

(41) Forlini, F.; Fan, Z.-Q.; Tritto, I.; Locatelli, P.; Sacchi, M. C. Metallocene-Catalyzed Propene/1-Hexene Copolymerization: Influence of Amount and Bulkiness of Cocatalyst and of Solvent Polarity. *Macromol. Chem. Phys.* **1997**, *198* (8), 2397–2408. https://doi.org/10.1002/macp.1997.021980804.

(42) Černý, Z.; Fusek, J.; Kříž, O.; Heřmánek, S.; Šolc, M.; Čásenský, B. 27Al NMR Study of the Trimethylaluminum Monomer-Dimer Equilibrium. *J. Organomet. Chem.* **1990**, *386* (2), 157–165.

https://doi.org/https://doi.org/10.1016/0022-328X(90)85240-Y.

(43) Babu, G. N.; Newmark, R. A.; Chien, J. C. W. *Microstructure of Poly(l-Hexene) Produced by Ansa-Zirconocenium Catalysis*; 1994; Vol. 27.

(44) Brintzinger, H. H.; Fischer, D.; Mülhaupt, R.; Rieger, B.; Waymouth, R. M. Stereospecific Olefin Polymerization with Chiral Metallocene Catalysts. *Angew. Chemie Int. Ed. English* **1995**, *34* (11), 1143–1170. https://doi.org/10.1002/anie.199511431.

(45) Lanzinger, D.; Höhlein, I. M.; Weiß, S. B.; Rieger, B. Catalytic C-F Activation via Cationic Group IV Metallocenes. *J. Organomet. Chem.* **2015**, *778*, 21–28. https://doi.org/10.1016/j.jorganchem.2014.12.011.

(46) Joshi, A.; Donnecke, S.; Granot, O.; Shin, D.; Collins, S.; Paci, I.; McIndoe, J. S. Gas-Phase Oxidation of Reactive Organometallic Ions. **2020**. https://doi.org/10.26434/CHEMRXIV.11909397.V1.

(47) Vikse, K. L.; Ahmadi, Z.; Luo, J.; van der Wal, N.; Daze, K.; Taylor, N.; McIndoe, J. S. Pressurized Sample Infusion: An Easily Calibrated, Low Volume Pumping System for ESI-MS Analysis of Reactions. *Int. J. Mass Spectrom.* **2012**, *323–324*, 8–13. https://doi.org/https://doi.org/10.1016/j.ijms.2012.03.007.

(48) Hesketh, A. V; Nowicki, S.; Baxter, K.; Stoddard, R. L.; McIndoe, J. S. Simplified Real-Time Mass Spectrometric Analysis of Reactions. *Organometallics* **2015**, *34* (15), 3816–3819. https://doi.org/10.1021/acs.organomet.5b00460.

(49) Bryliakov, K. P.; Talsi, E. P.; Voskoboynikov, A. Z.; Lancaster, S. J.; Bochmann, M. Formation and Structures of Hafnocene Complexes in MAO- and AlBui3/CPh3[B(C6F5)4]-Activated Systems. *Organometallics* **2008**, *27* (23), 6333–6342. https://doi.org/10.1021/om800664p.

(50) Pike, S. D.; Crimmin, M. R.; Chaplin, A. B. Organometallic Chemistry Using Partially Fluorinated Benzenes. *Chem. Commun.* **2017**, *53* (26), 3615–3633. https://doi.org/10.1039/c6cc09575e.

(51) Al-Humydi, A.; Youngs, W. J.; Collins, S. Propene Polymerization Using Ansa-Metallocenium Ions: Excess Activator Effects on Polymerization Activity and Polymer Microstructure. *Organometallics* **2005**, *24* (7), 1784. https://doi.org/10.1021/om050100j.

(52) Götz, C.; Rau, A.; Luft, G. Ternary Metallocene Catalyst Systems Based on Metallocene Dichlorides and AlBu3i/[PhNMe2H][B(C6F5)4]: NMR Investigations of the Influence of Al/Zr Ratios on Alkylation and on Formation of the Precursor of the Active Metallocene Species. *J. Mol. Catal. A Chem.* **2002**, *184* (1), 95–110. https://doi.org/https://doi.org/10.1016/S1381-1169(01)00517-9.

(53) Downs, A. J.; Greene, T. M.; Collin, S. E.; Whitehurst, L. A.; Brain, P. T.; Morrison, C. A.; Pulham, C. R.; Smart, B. A.; Rankin, D. W. H.; Keys, A.; et al. Dimethylalane, [Me2AlH]n, in the Vapor Phase and in Hydrocarbon Solution: Gas-Phase Electron Diffraction, Spectroscopic, Colligative, and Ab Initio Studies. *Organometallics* **2000**, *19* (4), 527–538. https://doi.org/10.1021/om990811f.

(54) Pankratyev, E. Y.; Khursan, S. L.; Tyumkina, T. V; Khalilov, L. M. A Quantum Chemical Study of Self-Association of HAlBu2iand ClAlBu2i. *J. Struct. Chem.* **2011**, *52* (1), 27–34. https://doi.org/10.1134/S0022476611010045.

(55) Busico, V.; Cipullo, R.; Romanelli, V.; Ronca, S.; Togrou, M. Reactivity of Secondary Metal−Alkyls in Catalytic Propene Polymerization: How Dormant Are “Dormant Chains”? *J. Am. Chem. Soc.* **2005**, *127* (6), 1608–1609. https://doi.org/10.1021/ja042839a.